Original Article

Image quality assessment and feasibility of three-dimensional amide proton transfer-weighted imaging for hepatocellular carcinoma

Xiaohui Qi[1], Qi Wang[1], Zhiwei Shen[2], Mengting Duan[1], Xiang Liu[1], Jiangyang Pan[1], Xueli Fan[1], Litao Jia[1], Yaning Wang[1], Yu Du[1]

[1]CT & MRI Department, The Fourth Hospital of Hebei Medical University, Shijiazhuang, China; [2]Philips (China) Investment Co., Ltd., Beijing, China

Contributions: (I) Conception and design: Q Wang, X Qi, Z Shen; (II) Administration support: None; (III) Provision of study materials or patients: M Duan, L Jia; (IV) Collection and assembly of data: X Liu, X Fan, Y Du; (V) Data analysis and interpretation: X Qi, J Pan; (VI) Manuscript writing: All authors; (VII) Final approval of manuscript: All authors.

Correspondence to: Qi Wang, MD. CT & MRI Department, The Fourth Hospital of Hebei Medical University, No. 12 Jiankang Road, Shijiazhuang, China. Email: Ja1109w@163.com.

Background: With the continuous innovation of magnetic resonance imaging (MRI) hardware and software technology, amide proton transfer-weighted (APTw) imaging has been applied in liver cancer. However, to our knowledge, no study has evaluated the feasibility of a three-dimensional amide proton transfer-weighted (3D-APTw) imaging sequence for hepatocellular carcinoma (HCC). This study thus aimed to conduct an image quality assessment of 3D-APTw for HCC and to explore its feasibility.

Methods: 3D-APTw MRI examinations were completed in 134 patients with clinically suspected HCC. According to the uniformity of APTw signal in the liver and within the lesion and the proportion of artifact and missing signal regions, APTw images were subjectively scored using a 5-point scale. The scanning success rate of liver APTw imaging was calculated as the ratio of the number of cases with a quality assurance measurement of more than 3 to the total number of HCC cases. The intra- and interobserver quality assurance measurements for APTw images were compared via the Kappa consistency test. Within the HCC cases with a minimum image quality threshold of 3 points, the APT values of HCC and the liver parenchyma, signal-to-noise ratio of APT-weighted images (SNR_{APTw}), and contrast-to-noise ratio of HCC (CNR_{HCC}) were measured by two observers. The intra- and interobserver agreement was assessed using the intraclass correlation coefficient (ICC). The differences in APT values between HCC and liver parenchyma was determined using the Mann-Whitney test.

Results: Sixty-six HCC cases with a quality assurance measurement of APTw imaging were included in the final analysis, and the calculated success rate was 70.21% (66/94). The subjective APT image quality scores of the two observers were consistent (3.66±1.18, 3.50±1.19, and 3.68±1.18), and no intergroup or intragroup statistical differences were found (P=0.594, and P=0.091), but the consistency of inter- and intraobserver was not as satisfactory (κ=0.594 and κ=0.580). The APT values in HCC lesion were significantly higher than those in liver parenchyma (2.73%±0.91% *vs.* 1.62%±0.55%; P<0.001). The APT values in HCC showed favorable intra- and interobserver consistency between the two observers (ICC =0.808 and ICC =0.853); the APT values in liver parenchyma, SNR_{APTw}, and CNRHCC values had moderate intraobserver consistency (ICC =0.578, ICC =0.568, and ICC =0.508) and interobserver consistency (ICC =0.599, ICC =0.199, and ICC =0.650). The coefficients of variation of the APTw values in the HCC lesion and in liver parenchyma were 33.4% and 34.4%, respectively. The SNR_{APTw} and CNRHCC were 30.75±18.74 and 3.56±3.19, with a coefficient of variation of 60.9% and 74.9%, respectively.

Conclusions: Liver 3D-APTw imaging was preliminarily demonstrated to be clinically feasible for evaluating HCC.

Keywords: Three-dimensional amide proton transfer-weighted imaging (3D-APTw imaging); hepatocellular carcinoma (HCC); diagnostic feasibility; image quality

Submitted May 30, 2023. Accepted for publication Jan 05, 2024. Published online Jan 23, 2024.
doi: 10.21037/qims-23-767
View this article at: https://dx.doi.org/10.21037/qims-23-767

Introduction

Primary hepatocellular carcinoma (HCC), the most common type of primary liver cancer, has a high incidence and an extremely high postoperative recurrence rate in China. Generally, recurrence within 3 years after surgery occurs in 40–50% of patients, and within 5 years after surgery occurs in 60–70% of patients. Therefore, preoperative and postoperative evaluation can contribute to effective intervention for patients with a high recurrence risk and may reduce the recurrence rate to achieve personalized medicine.

The assessment of preoperative factors and the prognostication of HCC recurrence are primarily based on the analysis of tumor pathological features (such as multiple tumors, satellite nodules, and lymph node metastasis) and serum tumor markers including alpha-fetoprotein (AFP). Additionally, imaging characteristics, such as the uptake of [^{18}F]fluorodeoxyglucose (^{18}F-FDG) and the presence of peritumoral microvascular invasion (MVI) based on computed tomography (CT) and magnetic resonance (MR) enhancement imaging, are also taken into consideration. The methods mentioned above, however, still have certain limitations, including a lack of sensitivity and specificity, the requirement for invasive injection of a contrast agent, and extensive postprocessing operations, which make clinical application challenging. Therefore, there is a need for a noninvasive imaging method that is able to provide molecular imaging or metabolic data to improve the accuracy of predicting the postoperative recurrence of HCC.

Amide proton transfer–weighted (APTw) imaging is a novel molecular MR imaging (MRI) technique based on the chemical exchange saturation transfer (CEST) effect. With APTw imaging, the magnetization transfer ratio asymmetry (MTRasym) between amide protons and water at 3.5 ppm can be measured to reflect the concentration characteristics and exchange environment (pH, temperature, etc.) of free proteins and polypeptides in tissue. Proteins rich in amide protons are not only components of cell structure but also the executors of cell function. Therefore, compared with information obtained from existing anatomical or diffusion imaging, weighted information on tumor proteins provided via APT imaging is more conducive to understanding the activity state of tumor cells (1,2) for efficacy evaluation and postoperative recurrence prediction. Studies in recent years have reported the application of APTw imaging in the prediction of the preoperative and postoperative recurrence of brain glioma and nasopharyngeal carcinoma (3-10), and some studies have explored the use of this technique in nonmotor organs outside the brain, such as the mammary gland, uterus, and prostate gland (11-14). A high APTw signal is positively correlated with the high-grade histopathological assignment, high cell counts and proliferation index, and thus this method can improve the sensitivity and specificity of tumor recurrence prediction. With the continuous innovation of magnetic resonance imaging (MRI) hardware and software technology, the application of APT imaging on liver cancer has been increasingly reported, and the possibility of applying APTw imaging in predicting the pathological grade of HCC has been proposed (15-18). Lin *et al.* published a study on the APTw of hepatic HCC with a single-shot turbo-spin-echo sequence on one slice and found that the APTw value of HCC was elevated (17). Seo *et al.* mainly assessed the feasibility using APT characteristics, also with a single-slice turbo spin-echo sequence, to characterize liver lesions (19). Therefore, it is reasonable to believe that liver APT imaging is expected to become a new tool for predicting HCC recurrence.

However, APTw imaging faces several technical challenges related to its application in the liver, as liver scanning can be easily affected by respiratory movement and heart beats. Previous studies on liver APT tended to adopt two-dimensional scanning, and the obtained images

Table 1 MRI scanning parameters

Sequence	Acquisition method	TR/TE (ms)	FOV (mm)	Matrix	Layer thickness/layer spacing (mm)	Number of layers	Times
T1WI	FFE-Dixon	3.1/1.12	400×350	448×448	4.5/−2.25	100	10
T2WI	MultiVane XD-TSE	1,800/85	380×380	640×640	6/1	30	170
DWI	EPI sequence	1,544/75	400×375	320×320	6/1	30	48
3D-APTw	Dixon-TSE	5,105/7.3	300×225	64×43	7/0	7	420
DCE	FFE-Dixon	3.1/1.12	400×340	512×512	6/−3	80	300

MRI, magnetic resonance imaging; TR, repetition time; TE, echo time; FFE, fast field echo; T1WI, T1-weighted imaging; T2WI, T2-weighted imaging; DWI, diffusion-weighted imaging; 3D-APTw, three-dimensional amide proton transfer–weighted; DCE, dynamic contrast-enhanced; FOV, field of vision; EPI, echo planar imaging; TSE, turbo spin echo.

were all single layer (17-19), making it difficult to reflect the APTw value and heterogeneity of the whole tumor. Moreover, according to our clinical findings, HCC is generally diagnosed in older adult patients who are in an advanced stage of the disease, and patient compliance is too poor during scanning to achieve regular breathing, which adversely affects the quality of APTw images. Philips has developed the 3D-APT technology for brain glioma imaging with automatic postprocessing and reconstruction in the scanner. However, to our knowledge, no study has been conducted to evaluate the feasibility of the 3D-APTw imaging sequence in clinical HCC scanning. As 3D-APT may be able to cover more lesions and is more conducive to clinical promotion, it is necessary to first conduct a study to assess the feasibility and quality of 3D-APT imaging for HCC.

In this study, we thus used a 3D-APT imaging sequence to measure the APTw signal of the lesion in a large sample of patients with HCC and completed a quality assurance measurement using objective indicators of image quality, which included the coefficient of variation (CV) of the signal-to-noise ratio (SNR) and contrast-to-noise ratio (CNR) of the lesion and peripheral liver tissues, the APTw values of the HCC and liver parenchyma, and inter- and intraobserver agreement. The ultimate aim of this study was to evaluate the image quality and feasibility of using 3D-APT imaging to examine HCC in clinic.

Methods

Study participants

This study prospectively enrolled 134 patients with clinically suspected or diagnosed liver tumor in The Fourth Hospital of Hebei Medical University from October 2020 to December 2021. The study was conducted in accordance with the Declaration of Helsinki (as revised in 2013) and was approved by the Ethics Committee of The Fourth Hospital of Hebei Medical University (No. 2021KY346). Written informed consent was obtained from the patients and their families.

The inclusion criteria for patients were as follows: (I) suspected diagnosis or diagnosis of HCC through CT or ultrasound; (II) no prior intervention, radiotherapy, or chemotherapy and no MRI contraindications; and (III) a lesion diameter ≥1.5 cm. Meanwhile, the exclusion criteria were as follows: (I) non-HCC diagnosis according to imaging or pathology (n=40; including 12 patients with hemangioma, 9 patients with metastases, 2 patients with abscess, and 17 patients with bile duct cell carcinoma or mixed HCC) and (II) a diffuse lesion.

MRI imaging technique

All patients were subjected to fasting for 6–8 hours prior to the MR examination. Patients were placed in a dorsal decubitus position and were scanned with a 3.0T MR system (Ingenia 3.0T CX, Philips, the Netherlands) with a 16-channel phased array body coil. Cross-sectional imaging was adopted for conventional liver MRI examination, including T1-weighted imaging (T1WI), T2-weighted imaging (T2WI), and diffusion-weighted imaging (DWI) (b value =1,200 s/mm^2). The scanning parameters are shown in *Table 1*. In 3D-APT imaging, fat suppression fast spin-echo sequence acquisition was repeatedly excited via spectral presaturation with inversion recovery (SPIR), and the Gaussian saturation pulse with alternating dual sources was used as the saturation method. T2WI was selected as the cross-sectional image to display the largest layer of the tumor. For patients with two or more lesions,

the largest one was selected for APT scanning. The tumor was covered in the field of vision (FOV) to the greatest extent. The optimized scanning parameters were as follows: matrix size =64×43; FOV =300×255 mm^2; saturation pulse power =2 μT; saturation duration =1.5 s; saturation offsets =±4.3, ±3.5, ±2.7, and −1,560 ppm; multishot excitation with turbo spin echo (TSE) factor =100; parallel acquisition sensitivity encoding (SENSE) =1; the phase-encoding direction, anterior to posterior; fold-over suppression, reassembled saturation transfer (REST); the number of signal acquisitions (NSA) =3 [with serial motion artifact reduction technique (SMART) averaging technique]; and imaging acquisition time, about 7 min. The patients received breathing training before scanning and were asked to complete a breath hold lasting several seconds when the machine sounded. The machine automatically generated B0 images through the Dixon method and automatically corrected B0 inhomogeneity. The scanner then automatically reconstructed the liver APTw images.

After APTw scanning, multiphase dynamic contrast-enhanced (DCE) images were also collected with the intravenous injection of 0.2 mL/kg gadoteric acid meglumine. After the enhancement of the aortic signal was observed for 3–5 min, the images of the liver's arterial phase, venous phase, and delayed phase were acquired. The parameters of DCE sequence are detailed in *Table 1*.

Image analysis

The analysis of APTw images was performed by two observers (with 5 and 15 years of experience in abdominal imaging diagnosis, respectively). The magnetization transfer ratio with asymmetric analysis (MTRasym; 3.5 ppm) images and B0 field inhomogeneous correction were automatically reconstructed on the scanner. The data postprocessing was performed with an IntelliSpace Portal workstation (ISP 9, Philips). After automatic and manual registration, MTRasym (3.5 ppm) images were fused on the T2W images to calculate the mean and SD of MTRasym (3.5 ppm) in lesion and liver tissue. Subjective scoring on the quality of APTw images was then performed. The numerical range of pseudocolor was set between −5% and 5%, with a signal greater than 8% in APTw images being regarded as an abnormally high signal and a possible artifact. The subjective scoring was based on the following a 5-point scale (20): 5 indicated uniform liver and lesion signals in the scanning range, with no artifacts and signal loss areas; 4 indicated artifacts or signal loss in the scanning range of the liver and lesion, with a range of <25% according to visual observation; 3 indicated a 25–50% range of artifacts and signal loss in the liver, with no artifacts or signal loss in the lesion; 2 indicated a 51–75% range of artifacts and signal loss in the liver or small artifacts or signal loss in the lesion; and 1 indicated a >75% range of artifacts and signal loss in the liver or large artifacts or signal loss in the lesion (*Figures 1*,*2*). The calculation method was as follows: success rate = number of cases with a quality assurance measurement of ≥3/number of HCC cases.

In the APT-T2WI fusion image, a region of interest (ROI) was drawn manually within the solid part of tumor in the largest lesion slice. Meanwhile, a distance of 1–2 mm was kept from the lesion edge with reference to the T2 image to reduce the interference of the partial volume effect. Several tissues with massive necrosis, calcification, hemorrhage, and large blood vessels, as well as the marginal area and artifacts with abnormally high signal ($MTRasym_{3.5\ ppm}$ >8%) in the lesion, were excluded within the ROI. Two other ROIs were then drawn in the lesion in the upper and lower layers, respectively. The average value of these three ROIs was calculated. In the liver parenchyma, three circular ROIs with an area of 200–700 mm^2 were also manually selected in the right lobe of the liver as the APT value of liver parenchyma, with large blood vessels and large artifacts being avoided (*Figure 3*). The average value of the three ROIs was also calculated. Finally, an objective assessment of image quality was performed.

The mean and standard deviation of APTw in the ROI of HCC tumor and in the ROI of liver parenchyma were measured on the nonsaturated M image with a saturation frequency of −1,560 ppm and the APTw image, respectively, and the mean value of three measurements was recorded, as described previously (21). Observer 1 performed a second measurement 1 week later.

The SNR of the APTw image (SNR_{APTw}) and the CNR of HCC (CNR_{HCC}) were calculated according to the following equations (21):

$$SNR_{I0} = \frac{Mean}{Standard\ deviation\ of\ the\ lesion\ on\ the\ M\ image} \quad [1]$$

$$SNR_{APTw} = \frac{APTw_{HCC}}{\sqrt{2 + APTw_{HCC}^2}} \times SNR_{I0} \quad [2]$$

$$CNR_{HCC} = \frac{APTw_{HCC} - APTw_{live\ parenchyam}}{\sqrt{SD_{HCC}^2 - SD_{live\ parenchyam}^2}} \times \frac{1}{\sqrt{TR \times NSA}} \quad [3]$$

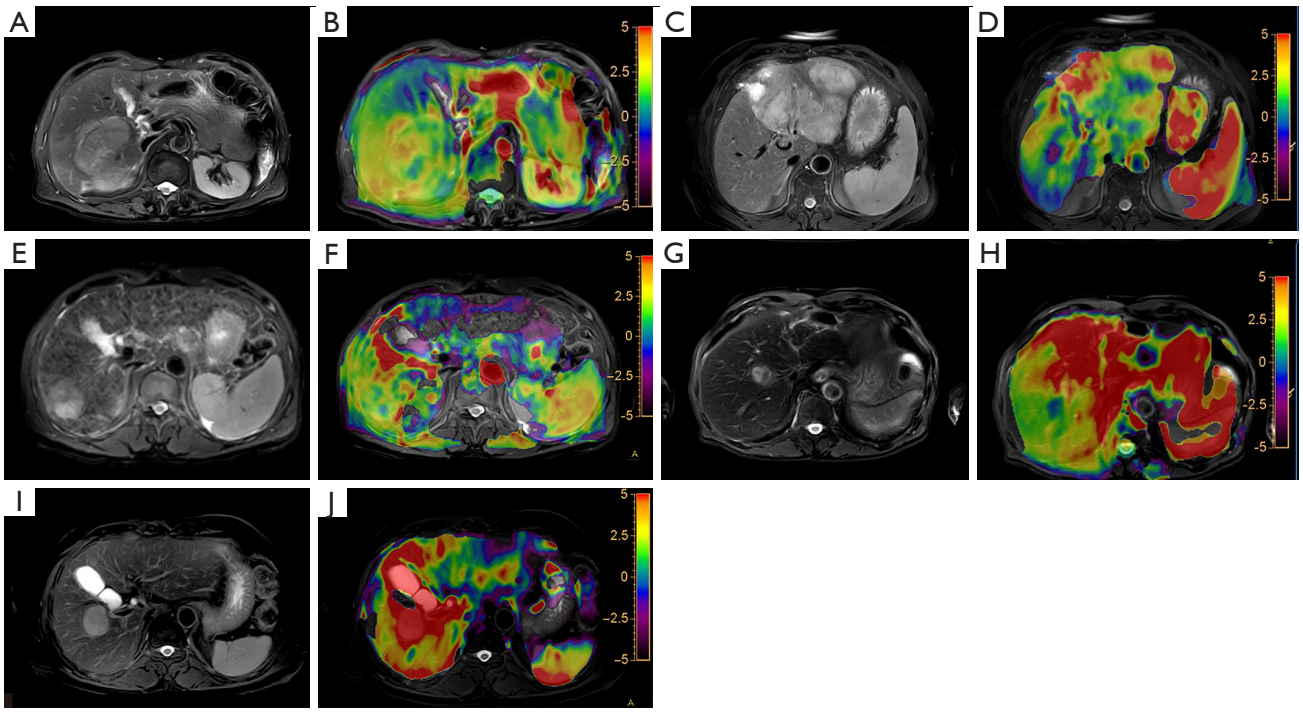

Figure 1 APTw images with quality assurance measurements. (A,C,E,G,I) T2WI image. (B,D,F,H,J) APTw–T2WI fusion image. (A,B) Uniform liver and lesion signals, with no artifacts and signal loss areas; the score was 5. (C,D) Artifacts in the liver and lesion with a range of <25% according to visual observation; the score was 4. (E,F) A signal loss range of about 25–50% in the left lobe of the liver and a uniform signal in the lesion with no artifacts or signal loss; the score was 3. (G,H) A 51–75% range of artifacts and signal loss in the liver; the score was 2. (I,J) An artifact range of above 75% in the liver, with large artifacts in the lesion; the score was 1. APTw, amide proton transfer–weighted; T2WI, T2-weighted imaging.

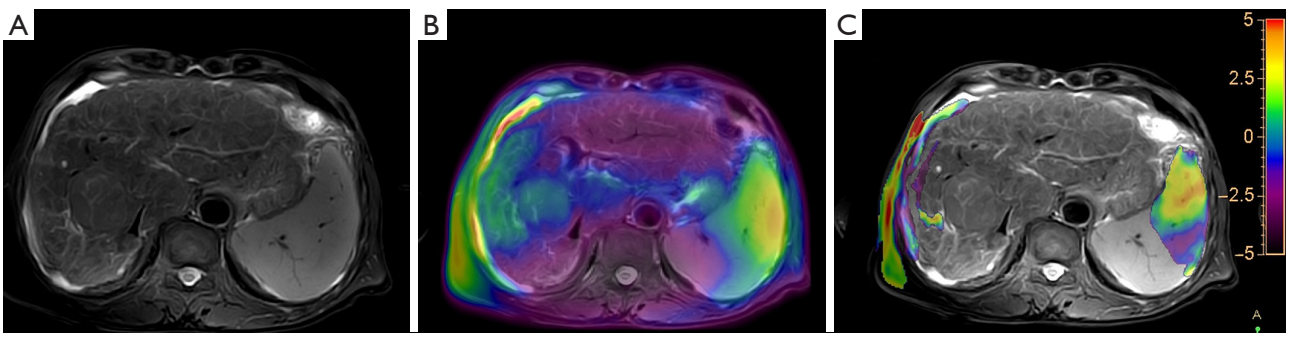

Figure 2 A case with scan failure. (A) T2WI, (B) M map, and (C) APTw map. (C) No APT signal appeared at the lesion level, but there was HCC in the right lobe of the liver. APTw, amide proton transfer-weighted; T2WI, T2-weighted imaging; HCC, hepatocellular carcinoma.

where $APTw_{HCC}$ is mean APTw of HCC, $APTw_{live\ parenchyam}$ is the mean APTw of liver parenchyma, SD_{HCC} is the standard deviation of the APTw value of HCC, $SD_{liver\ parenchyma}$ is the standard deviation of the APTw value of liver parenchyma, TR is 5.1, and NSA is 3.

Statistical analysis

Statistical analysis was performed using SPSS 25.0 for Windows (IBM Corp.) and MedCalc 15.6.1 (MedCalc Software). The quality assurance measurement, SNR, and CNR are expressed as the mean ± standard deviation. The

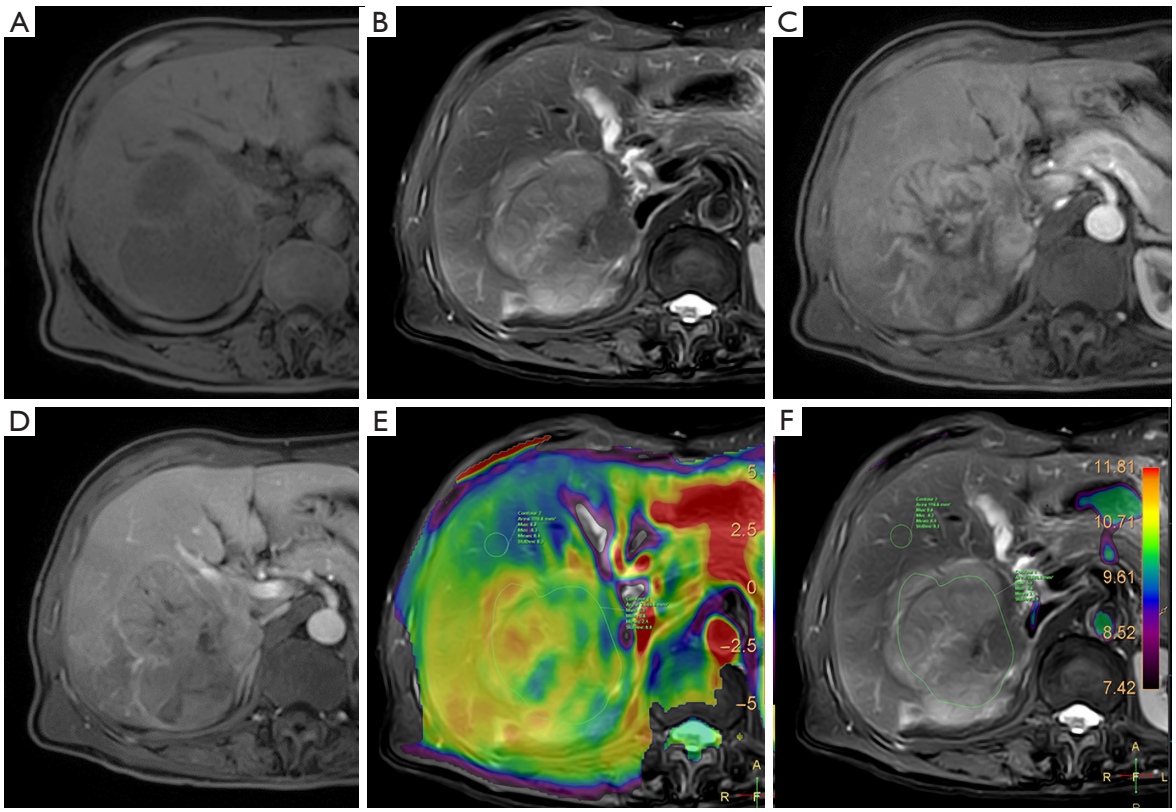

Figure 3 A 66-year-old man with HCC. (A-E) T1WI, T2WI, arterial image, venous image, and APTw image, respectively. The APT value of HCC was 2.1%, and the APTw value of liver parenchyma was 0.4%. (E,F) The ROI drawn along the tumor margin. HCC, hepatocellular carcinoma; T1WI, T1-weighted imaging; T2WI, T2-weighted imaging; APTw, amide proton transfer-weighted; ROI, region of interest.

CV of the SNR_{APTw}, CNR_{HCC}, and APTw values of HCC and liver parenchyma were calculated. The Kappa consistency test was used to analyze the consistency of the intra- and interobserver quality assurance measurements. $\kappa \geq 0.75$ indicated high consistency, κ between 0.4 and 0.75 indicated moderate consistency, and $\kappa < 0.4$ indicated poor consistency. The consistency between and within the two observers was analyzed by calculating the intraclass correlation coefficient (ICC) values for the SNR_{APTw}, CNR_{HCC}, and APTw values of HCC and liver parenchyma. ICC >0.75 indicated high consistency, ICC between 0.60 and 0.74 indicated good consistency; ICC between 0.40 and 0.59 indicated moderate consistency, and ICC <0.40 indicated poor consistency. The Mann-Whitney test (nonparametric rank-sum test) for two independent samples was performed to determine whether there was any difference between the APT values of HCC and liver parenchyma. A P value <0.05 was considered to be a statistically significant difference. The agreement between intraobserver and interobserver measurements of HCC APTw, liver parenchyma APTw, SNR_{APTw}, and CNR_{HCC} was obtained using Bland-Altman plots.

Results

APTw images of 94 cases of primary HCC confirmed by pathology or diagnosed by imaging (based on the 2019 Chinese Guidelines for the Diagnosis and Treatment of Hepatocellular Carcinoma) were included for analysis. There were 73 males and 21 females (mean age 59.78±11.63 years; age range 19–87 years). Among the 94 patients, 11 had an APTw image showing no lesion signal or no lesion within the scanning range. Among these patients, eight had a lesion located on the liver margin, two had no lesion within the scanning range, and one had no signal in most of the scanning area (*Figure 4*).

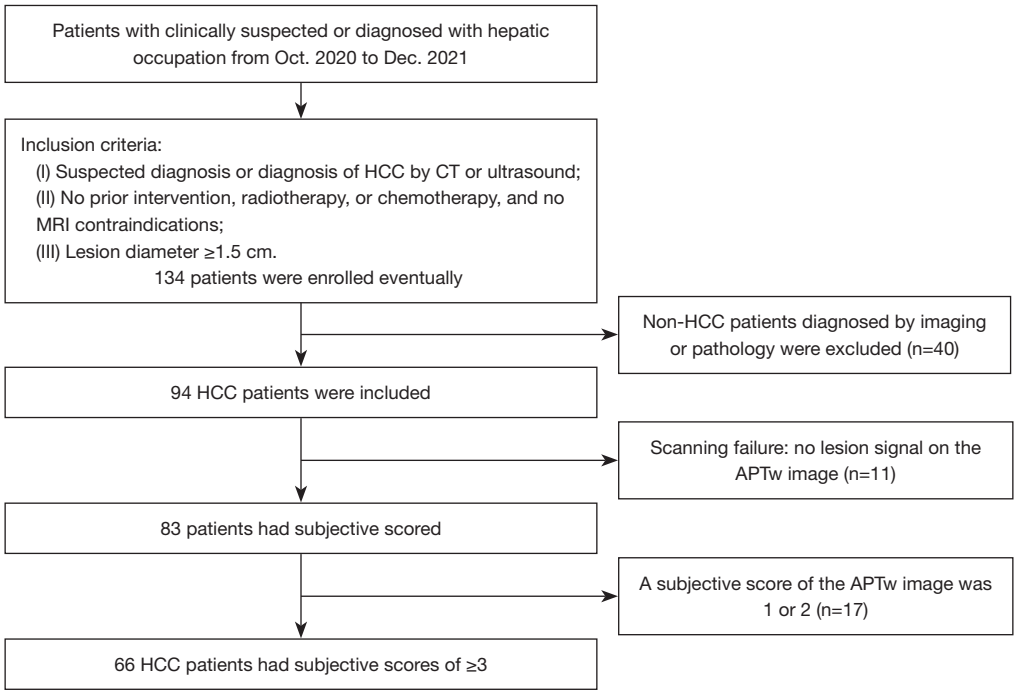

Figure 4 Patient selection flowchart. HCC, hepatocellular carcinoma; CT, computed tomography; MRI, magnetic resonance imaging; APTw, amide proton transfer-weighted.

Quality assurance measurement

The APTw images of 83 patients (*Table 2*) were analyzed and subjectively scored. The clinical information is listed in *Table 1*. The scores of physician 1 twice and physician 2 were 3.66±1.18, 3.50±1.19, and 3.68±1.18. There was no statistical difference in the quality assurance measurement between (chi-squared value =3.69; P=0.594) or within the observers (chi-squared value =9.5; P=0.091), but the consistency of the intra- and interobserver quality assurance measurements was not as satisfactory, with the κ values being 0.594 and 0.580, respectively (P<0.001). The APTw images of 17 patients had a quality assurance measurement score of 1 or 2; the lesion was located at the apex of the liver in 7 patients, near the gallbladder or the large blood vessel of the liver in 6 patients, and on the liver margin in 4 patients. As 66 patients had a quality assurance measurement score for the APTw image of ≥3, the calculated success rate was 70.21% (66/94).

APTw values, CVs, SNR, and CNR of HCC lesion and liver parenchyma with a quality assurance measurement score ≥3

In order to measure the APTw values of HCC lesion and liver parenchyma, 66 patients were included in the success group, including 52 males and 14 females, with a mean age of 59.9±11.6 years (range, 19–87 years). The maximum lesion diameter was 6.86±4 cm (range, 2–19 cm). The APTw values in the HCC lesion were significantly greater than those observed in the liver parenchyma (Z=−6.903; P<0.001) (*Figure 5*, *Table 3*). The CV of the APTw values of the HCC and liver parenchyma was 33.4% and 34.4%, respectively. The SNR_{APTw} was 30.75±18.74, with a CV of 60.9%, and the CNR_{HCC} was 3.56±3.19, with a CV of 74.9% (*Table 3*).

Consistency analysis of the HCC APTw values, SNRAPTw, and CNRHCC

The Bland-Altman plots demonstrated that the APTw value of HCC exhibited a high level of inter- and intraobserver consistency. Similarly, the APTw value of liver parenchyma, SNR_{APTw}, and CNR_{HCC} also displayed a satisfactory level of inter- and intraobserver consistency (*Table 4* and *Figure 6*).

Discussion

This study was the first of its kind to assess the feasibility

Table 2 Clinical information of patients with a successful scan (n=83)

Clinical information	No. of patients (%) or mean ± SD
Age (years)	59.78±11.63
Sex	
Male	66 (79.52)
Female	17 (20.48)
Etiology	
HBV	78 (93.98)
HCV	5 (6.02)
Child stage	
A	61 (73.49)
B	15 (18.07)
C	7 (8.43)
AFP level, ng/mL	
<400	51 (61.45)
400–1,210	11 (13.25)
>1,210	21 (25.30)
Number of tumor(s)	
1	66 (79.52)
2	6 (7.23)
>2	11 (13.25)
Tumor site	
Left lobe	16 (19.28)
Right lobe	59 (71.08)
Caudal lobe	1 (1.20)
>2 lobes	7 (8.43)
Treatment method	
Surgical excision	54 (65.06)
TACE or ablation	20 (24.10)
Chemotherapy or targeted immunotherapy	9 (10.84)

SD, standard deviation; HBV, hepatitis B virus; HCV, hepatitis C virus; AFP, alpha-fetoprotein; TACE, transcatheter arterial chemoembolization.

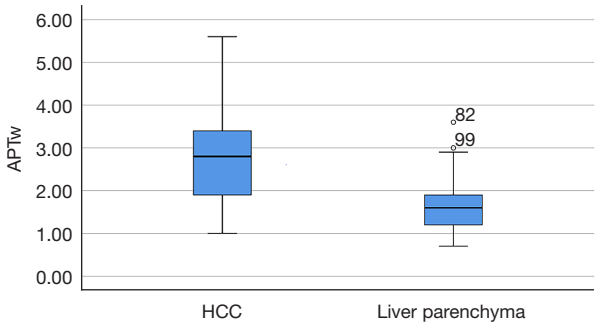

Figure 5 Comparison of APTw values between HCC and liver parenchyma. HCC, hepatocellular carcinoma; APTw, amide proton transfer-weighted.

of a 3D-APTw imaging sequence in HCC scanning, and the results showed that the success rate of liver 3D-APT imaging was 70.21%, which was higher than that of a previous study (62.1%) (20). There was no statistical difference in the quality assurance measurement of image quality between and within the two observers. The APT value was higher for HCC than for liver parenchyma, and the difference between them was statistically significant. In addition, the measurement repeatability of the HCC APTw value was high, but the repeated measurement consistency of liver parenchyma APTw, SNR, and CNR was moderate, as the ICC values only ranged from 0.5 to 0.6.

Previous studies on the feasibility of APT imaging in liver scanning and tumor diagnosis (16,22) generally adopted 2D scanning, which could only acquire single-layer images and had a relatively low success rate. In the study by Seo *et al.* (19), the success rate of 2D-APT imaging for liver scanning was only 62.1%, with about one-third of the patients experiencing scanning failure due to B0 heterogeneity and the influence of respiratory movement. In terms of success rate, the results of this study represent a significant advancement over previous studies, likely due to the use of 3D scanning in this study (the scanning range was large, which reduced the impact of respiratory movement to some extent) and more up-to-date machine hardware and software. These are the advantages of 3D-APTw imaging in the scanning of HCC or liver lesions.

However, although there was no statistical difference in the quality assurance measurement of image quality between and within the two observers, the consistency of the results was moderate. Moreover, signal loss was observed in the lesion area of some patients. The main factor leading to scanning failure could be attributed to lesions located in the marginal region of the liver, which tended to be affected by the heterogeneity of the B0 magnetic field, air, or ribs, despite the machine automatically generating images for which B0 heterogeneity had been corrected.

As revealed by our analysis of the APTw images from

Table 3 SNR_{APTw}, CNR_{HCC}, and APTw values of HCC and liver parenchyma

Indicator	SNR_{APTw}	CNR_{HCC}	APTw value of HCC (%)	APTw value of liver parenchyma (%)	Z	P*
Mean ± SD	30.75±18.74	3.56±3.19	2.73±0.91	1.62±0.55	−6.903	<0.001
CV	60.9%	74.9%	33.4	34.4		

*, P value is the result of the APTw value comparison between HCC and liver parenchyma. SNR_{APTw}, signal-to-noise ratio of APTw imaging; CNR_{HCC}, contrast-to-noise ratio of HCC; HCC, hepatocellular carcinoma; APTw, amide proton transfer-weighted; SD, standard deviation; CV, coefficient of variation.

Table 4 Intra- and interobserver consistency of HCC APTw value, liver parenchyma APTw value, SNR_{APTw}, and CNR_{HCC}

Indicator	ICC	95% CI	
		Lower bound	Upper bound
Intraobserver consistency			
APTw value of HCC	0.808	0.694	0.880
APTw value of liver parenchyma	0.578	0.394	0.718
SNR_{APTw}	0.568	0.381	0.711
CNR_{HCC}	0.508	0.314	0.661
Interobserver consistency			
APTw value of HCC	0.853	0.775	0.906
APTw value of liver parenchyma	0.599	0.427	0.729
SNR_{APTw}	0.199	−0.03	0.412
CNR_{HCC}	0.650	0.484	0.770

HCC, hepatocellular carcinoma; APTw, amide proton transfer–weighted; SNR_{APTw}, signal-to-noise ratio of APTw imaging; CNR_{HCC}, contrast-to-noise ratio of HCC; ICC, intraclass correlation coefficient; CI, confidence interval.

patients with successful scans, 20.48% of the patients had a signal loss of varying degrees or high signal artifacts in the liver parenchyma and lesion, with a higher incidence and a greater proportion in areas at the liver margin, near the gallbladder, or near the large blood vessel. This phenomenon could be the result of the excessive exchange between water and amide protons (e.g., proteins and peptides in blood, cytoplasm, or other body fluids) or of the interference from the nuclear Overhauser effect and conventional magnetization transfer effect which can contribute to high APT signals (20). Alternatively, the portal system and hepatic artery in the liver with a high APTw value (16) can extend to tumor tissues or liver parenchyma near the blood vessels and produce high signal artifacts. Areas with hemorrhage and necrosis in the lesion might also respond with high signals and APTw values. As these artifacts might have caused interference in ROI delineation and compromise the accuracy of data measurement, we identified them with reference to anatomical images and avoided these areas during ROI drawing and data measurement to reduce measurement errors.

We further found that the APT value was significantly higher in HCC than in liver parenchyma. This is consistent with the findings of APT in other tumors (23-29), including glioma, prostate cancer, rectal cancer, endometrial cancer, and cervical cancer. According to previous studies, a high APT value is associated with a high cell proliferation rate and is positively correlated with the pathological grade of HCC. An increase in the APT value of HCC tissue is likely to be caused by a markedly elevated content of protein or polypeptide in the tumor due to vigorous cell division and proliferation in HCC tissue or by the more frequent exchange of amino acid protons and free water protons in liver cancer tissue resulting from changes in the tumor microenvironment (where cancer cells are produced) due to active HCC tissue cells. In the study by Jia *et al.* (30), the APTw value of liver parenchyma distant from the HCC lesion was 2.73%±0.91%, while in our study, the APTw

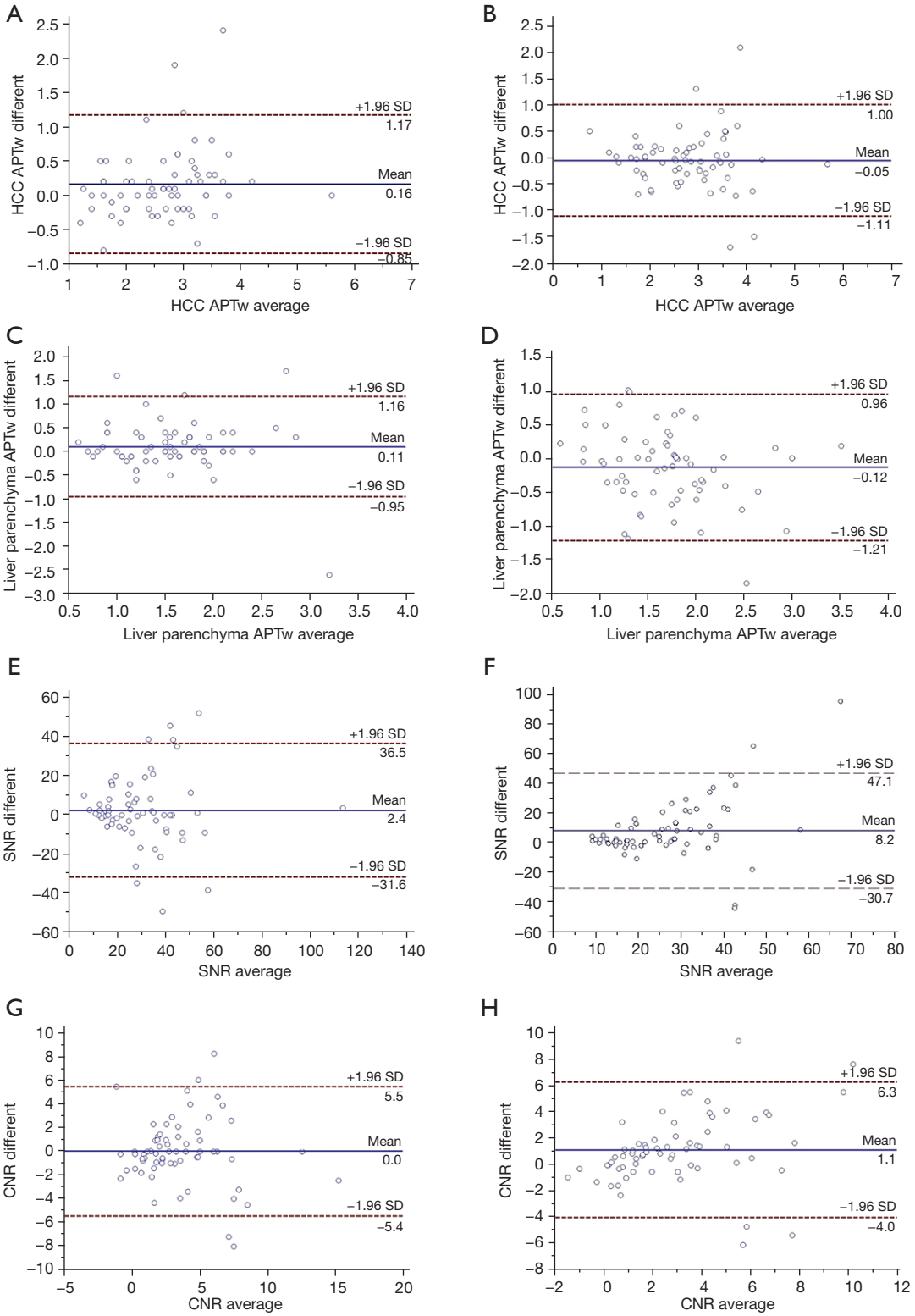

Figure 6 Intra- and interobserver consistency of the HCC APTw value, liver parenchyma APTw value, SNR_{APTw}, and CNR_{HCC}. HCC, hepatocellular carcinoma; APTw, amide proton transfer-weighted; SNR_{APTw}, signal-to-noise ratio of APTw imaging; CNR_{HCC}, contrast-to-noise ratio of HCC.

value of the liver parenchyma in liver cirrhosis measured was lower, at 1.62%±0.55%. The possible explanations for this may be as follows: the parameters used for APT imaging (e.g., saturation intensity, saturation period, and magnetic field heterogeneity) in this study were different from those in the previous study; the images obtained in this study were 3D, which means that the measured values were the mean liver parenchyma APTw values of three perspectives, while the images in the previous study consisted of only a single layer; furthermore, the degree of liver cirrhosis and fibrosis also could have affected the final outcome.

Chen *et al.* (16) were the first to evaluate the repeatability of 3.0T MRI APTw imaging in the scanning of rat and human livers, and their results showed that APT imaging had good repeatability between two scans in healthy volunteers. This study also produced a high measurement repeatability for HCC APTw value, but the consistency of repeated measurements for liver parenchyma APTw, SNR_{APTw}, and CNR_{HCC} was moderate. This result may be linked to the patients included in this study. Since the patients all had HCC with liver cirrhosis, their breathing amplitude and rhythm were less stable compared to those healthy volunteers, and the degree of cirrhosis could have affected the stability of the liver parenchyma APTw value. Additionally, liver parenchyma APTw values can be easily altered by intrahepatic blood vessels, bile ducts, adjacent gallbladder, or artifacts. The measurement results were also related to the location and size of the ROI. The CVs of SNR of liver APT image sand of HCC CNR were high in this study, and the results varied widely across different patients, which could be related to the varying degrees of cirrhosis and pathological grades of HCC.

Despite the promising findings, this study involved some limitations that should be addressed. First, this study was limited to the feasibility of APTw imaging in the scanning and diagnosis of HCC, with no other tumors being examined. In the future, we will further investigate the value of APTw imaging in the diagnosis and differential diagnosis of liver neoplastic lesions. Second, liver APTw imaging is still in its initial stage. In some cases of this study, APTw imaging was easily affected by motion artifacts, gallbladder, or blood circulation, which led to heavy artifacts or signal loss on the images. Further improvement is required in the APTw imaging technique or parameter setting. Third, the MRI signal and enhancement characteristics were not analyzed in this study nor was the impact of HCC pathological grade on the APTw value of the tumor. We will next investigate the correlation between the APTw value, MRI signal, enhancement characteristics, and the pathological features of HCC.

Conclusions

The scanning success rate of the 3D-APTw imaging technique was greatly improvement compared to 2D-APTw in HCC patients, and high measurement repeatability and high consistency of APTw values were achieved in HCC lesions. As an emerging molecular imaging technique, 3D-APTw imaging has broad application prospects in the diagnosis of liver tumors. It can be applied to examine HCC and may serve as a reliable and productive technical foundation for further exploration of this technology in the diagnosis and prognostic prediction of HCC.

Acknowledgments

Funding: None.

Footnote

Conflicts of Interest: All authors have completed the ICMJE uniform disclosure form (available at https://qims.amegroups.com/article/view/10.21037/qims-23-767/coif). Z.S. is the employee of Philips (China) Investment Co., Ltd, but he had no control over inclusion of any data or information that might have presented a conflict of interest; thus, there are no actual or potential conflicts of interest to declare in relation to this study. The other authors have no conflicts of interest to declare.

Ethical Statement: The authors are accountable for all aspects of the work in ensuring that questions related to the accuracy or integrity of any part of the work are appropriately investigated and resolved. This study was conducted in accordance with the Declaration of Helsinki (as revised in 2013) and was approved by the Ethics Committee of The Fourth Hospital of Hebei Medical University (No. 2021KY346). Written informed consent was obtained from the patients and their families.

References

1. Kamimura K, Nakajo M, Yoneyama T, Takumi K, Kumagae Y, Fukukura Y, Yoshiura T. Amide proton transfer imaging of tumors: theory, clinical applications, pitfalls, and future directions. Jpn J Radiol 2019;37:109-16.
2. Liu N. Advancement in the Application of Amide Proton Transfer Imaging in Tumor Imaging. Journal of Practical Medical Imaging 2020;21:50-2.
3. Park JE, Kim HS, Park SY, Jung SC, Kim JH, Heo HY. Identification of Early Response to Anti-Angiogenic Therapy in Recurrent Glioblastoma: Amide Proton Transfer-weighted and Perfusion-weighted MRI compared with Diffusion-weighted MRI. Radiology 2020;295:397-406.
4. Jiang S, Eberhart CG, Lim M, Heo HY, Zhang Y, Blair L, Wen Z, Holdhoff M, Lin D, Huang P, Qin H, Quinones-Hinojosa A, Weingart JD, Barker PB, Pomper MG, Laterra J, van Zijl PCM, Blakeley JO, Zhou J. Identifying Recurrent Malignant Glioma after Treatment Using Amide Proton Transfer-Weighted MR Imaging: A Validation Study with Image-Guided Stereotactic Biopsy. Clin Cancer Res 2019;25:552-61.
5. Joo B, Han K, Choi YS, Lee SK, Ahn SS, Chang JH, Kang SG, Kim SH, Zhou J. Amide proton transfer imaging for differentiation of benign and atypical meningiomas. Eur Radiol 2018;28:331-9.
6. Zhang J, Zhu W, Tain R, Zhou XJ, Cai K. Improved Differentiation of Low-Grade and High-Grade Gliomas and Detection of Tumor Proliferation Using APT Contrast Fitted from Z-Spectrum. Mol Imaging Biol 2018;20:623-31.
7. Yu L, Li C, Luo X, Zhou J, Zhang C, Zhang Y, Chen M. Differentiation of Malignant and Benign Head and Neck Tumors with Amide Proton Transfer-Weighted MR Imaging. Mol Imaging Biol 2019;21:348-55.
8. Mehrabian H, Desmond KL, Soliman H, Sahgal A, Stanisz GJ. Differentiation between Radiation Necrosis and Tumor Progression Using Chemical Exchange Saturation Transfer. Clin Cancer Res 2017;23:3667-75.
9. Choi YS, Ahn SS, Lee SK, Chang JH, Kang SG, Kim SH, Zhou J. Amide proton transfer imaging to discriminate between low- and high-grade gliomas: added value to apparent diffusion coefficient and relative cerebral blood volume. Eur Radiol 2017;27:3181-9.
10. Zhou J, Heo HY, Knutsson L, van Zijl PCM, Jiang S. APT-weighted MRI: Techniques, current neuro applications, and challenging issues. J Magn Reson Imaging 2019;50:347-64.
11. Takayama Y, Nishie A, Togao O, Asayama Y, Ishigami K, Ushijima Y, Okamoto D, Fujita N, Sonoda K, Hida T, Ohishi Y, Keupp J, Honda H. Amide Proton Transfer MR Imaging of Endometrioid Endometrial Adenocarcinoma: Association with Histologic Grade. Radiology 2018;286:909-17.
12. Li B, Sun H, Zhang S, Wang X, Guo Q. Amide proton transfer imaging to evaluate the grading of squamous cell carcinoma of the cervix: A comparative study using 18 F FDG PET. J Magn Reson Imaging 2019;50:261-8.
13. Nishie A, Takayama Y, Asayama Y, Ishigami K, Ushijima Y, Okamoto D, Fujita N, Tsurumaru D, Togao O, Manabe T, Oki E, Kubo Y, Hida T, Hirahashi-Fujiwara M, Keupp J, Honda H. Amide proton transfer imaging can predict tumor grade in rectal cancer. Magn Reson Imaging 2018;51:96-103.
14. Nishie A, Asayama Y, Ishigami K, Ushijima Y, Takayama Y, Okamoto D, Fujita N, Tsurumaru D, Togao O, Sagiyama K, Manabe T, Oki E, Kubo Y, Hida T, Hirahashi-Fujiwara M, Keupp J, Honda H. Amide proton transfer imaging to predict tumor response to neoadjuvant chemotherapy in locally advanced rectal cancer. J Gastroenterol Hepatol 2019;34:140-6.
15. Wáng YXJ, Dou W, Shen Z, Zhang Y. An update on liver chemical exchange saturation transfer imaging with a focus on clinical translation. Quant Imaging Med Surg 2023;13:4057-76.
16. Chen SZ, Yuan J, Deng M, Wei J, Zhou J, Wáng YX. Chemical exchange saturation transfer (CEST) MR technique for in-vivo liver imaging at 3.0 tesla. Eur Radiol 2016;26:1792-800.
17. Lin Y, Luo X, Yu L, Zhang Y, Zhou J, Jiang Y, Zhang C, Zhang J, Li C, Chen M. Amide proton transfer-weighted MRI for predicting histological grade of hepatocellular carcinoma: comparison with diffusion-weighted imaging. Quant Imaging Med Surg 2019;9:1641-51.
18. Wu B, Jia F, Li X, Li L, Wang K, Han D. Comparative Study of Amide Proton Transfer Imaging and Intravoxel Incoherent Motion Imaging for Predicting Histologic Grade of Hepatocellular Carcinoma. Front Oncol 2020;10:562049.
19. Seo N, Jeong HK, Choi JY, Park MS, Kim MJ, Chung YE. Liver MRI with amide proton transfer imaging: feasibility

and accuracy for the characterization of focal liver lesions. Eur Radiol 2021;31:222-31.
20. Chen Y, Wang X, Su T, Xu Z, Wang Y, Zhang Z, Xue H, Zhuo Z, Zhu Y, Jin Z, Zhang T. Feasibility evaluation of amide proton transfer-weighted imaging in the parotid glands: a strategy to recognize artifacts and measure APT value. Quant Imaging Med Surg 2021;11:2279-91.
21. Kim J, Wu Y, Guo Y, Zheng H, Sun PZ. A review of optimization and quantification techniques for chemical exchange saturation transfer (CEST) MRI toward sensitive in vivo imaging. Contrast Media Mol Imaging 2015;10:163-78.
22. Deng M, Chen SZ, Yuan J, Chan Q, Zhou J, Wáng YX. Chemical Exchange Saturation Transfer (CEST) MR Technique for Liver Imaging at 3.0 Tesla: an Evaluation of Different Offset Number and an After-Meal and Over-Night-Fast Comparison. Mol Imaging Biol 2016;18:274-82.
23. Zhao J, Huang S, Xie H, Li W. An evidence-based approach to evaluate the accuracy of amide proton transfer-weighted MRI in characterization of gliomas. Medicine (Baltimore) 2019;98:e14768.
24. Chen Y, Li X, Song Y, Zhu X, Zhao J, Yan X, Wang J, Fan M, Chu J. The diagnostic efficacy of amide proton transfer imaging in grading gliomas and predicting tumor proliferation. Neuroreport 2019;30:139-44.
25. Li G, Jiang G, Mei Y, Gao P, Liu R, Jiang M, Zhao Y, Li M, Wu Y, Fu S, Liu M, Li L, Li W, Yan J. Applying Amide Proton Transfer-Weighted Imaging (APTWI) to Distinguish Papillary Thyroid Carcinomas and Predominantly Solid Adenomatous Nodules: Comparison With Diffusion-Weighted Imaging. Front Oncol 2020;10:918.
26. Meng N, Wang J, Sun J, Liu W, Wang X, Yan M, Dwivedi A, Zheng D, Wang K, Han D. Using amide proton transfer to identify cervical squamous carcinoma/adenocarcinoma and evaluate its differentiation grade. Magn Reson Imaging 2019;61:9-15.
27. Yang L, Wang L, Tan Y, Dan H, Xian P, Zhang Y, Tan Y, Lin M, Zhang J. Amide Proton Transfer-weighted MRI combined with serum prostate-specific antigen levels for differentiating malignant prostate lesions from benign prostate lesions: a retrospective cohort study. Cancer Imaging 2023;23:3.
28. Yin HJ, Yan RF, Ren JP, Ren JP, Zhou FM, Meng N, Han DM. Diagnostic Value of Amide Proton Transfer (APT) Magnetic Resonance Imaging for Prostate Cancer. Journal of Clinical Radiology 2019;38:1698-702.
29. Meng N, Wang X, Sun J, Huang Z, Yang Z, Shang J, Bai Y, Wei W, Han D, Han H, Wang K, Shao F, Wang M. Evaluation of amide proton transfer-weighted imaging for endometrial carcinoma histological features: a comparative study with diffusion kurtosis imaging. Eur Radiol 2021;31:8388-98.
30. Jia F, Meng N, Wu BL, Yin HJ, Hou MY, Han DM. Diagnosis Value of Amide Proton Transfer Imaging for Primary Hepatocellular Carcinoma. Chinese Medical Equipment Journal 2020;41:51-5.

Cite this article as: Qi X, Wang Q, Shen Z, Duan M, Liu X, Pan J, Fan X, Jia L, Wang Y, Du Y. Image quality assessment and feasibility of three-dimensional amide proton transfer-weighted imaging for hepatocellular carcinoma. Quant Imaging Med Surg 2024;14(2):1778-1790. doi: 10.21037/qims-23-767

